The charge densities and the electric field lines are represented in Fig. 8. As can be seen, in the case of the second-type modes, we also get a quasi-quadrupole oscillation on the separating wall. Here, again, the influence of the curvature of the torus appears.

V. Conclusions

The paper contains the solution of Maxwell's equations for a torus with a separating wall. We think that the great advantage of the described solution is that it is an exact one for a complicated geometry, and no approximations were used anywhere.

The special symmetry of the torus with a separating wall does not allow the simple E and H classification of the waves. Therefore, we had to introduce a different classification, which was dictated by our mathematical method.

Acknowledgment

The author acknowledges the support by the Österreichischer Fonds zur Förderung der wissenschaftlichen Forschung. He would also like to express his gratitude to Prof. F. Cap for useful discussions during the elaboration of this paper.

References

[1] F. Cap and R. Deutsch, "Toroidal electromagnetic modes in isotropic homogeneous plasma and in vacuum," presented at the 3rd Int. Congress on Waves and Instabilities in Plasmas, Paris, France, June 27–July 2, 1977.

[2] ——, "Toroidal resonators for electromagnetic waves," *IEEE Trans. Microwave Theory Tech.*, vol. MTT-26, pp. 478–486, July 1978.

[3] R. Deutsch, "Toroidal electromagnetic modes in a torus containing plasma and in coaxial toroidal systems," to be published.

[4] Jahnke, Emde, and Lösch, *Tables of Higher Functions*. Stuttgart, Germany: B. G. Teubner Verlagsgesellschaft, 1960.

Characteristics and Optimum Operating Parameters of a Gyrotron Traveling Wave Amplifier

KWO RAY CHU, ADAM T. DROBOT, VICTOR L. GRANATSTEIN, AND J. LARRY SEFTOR

Abstract—**Characteristics and optimum operating parameters are determined for a new type of high-power high-efficiency generator of millimeter waves known as a gyrotron traveling wave amplifier. In the example considered, wave amplification results from the interaction of a TE_{01} waveguide mode with the fundamental cyclotron harmonic of an electron beam. The parameter optimization involves the determination of the point of maximum device efficiency as a function of beam density, beam energy, beam positioning, and external magnetic field for the output power required. An analytical linear theory and a numerical simulation code form the basis of theoretical calculations. As a result of the extensive survey in parameter space, the peak efficiency in the beam frame has been found to exceed 70 percent. This result has been applied to the specific design of a 35-GHz amplifier with output power ~340 kW, a power gain of 2 dB/cm, and a laboratory frame efficiency of 51 percent.**

Manuscript received October 7, 1977; revised May 11, 1978. This work was supported in part by the Naval Electronic Systems Command, Task XF 54-587, by the Army Ballistic Missile Defense Advanced Technology Center, MIPR W31RPD-73-Z787, and by the Naval Surface Weapons Center (Dahlgren), Task SF32-302-41B.

K. R. Chu was with Science Applications, Inc., McLean, VA. He is now with the Plasma Physics Division, Naval Research Laboratory, Washington, DC 20375.

A. T. Drobot is with Science Applications, Inc., McLean, VA 22101.

V. L. Granatstein and J. L. Seftor are with the Plasma Physics Division, Naval Research Laboratory, Washington, DC 20375.

I. Introduction

THE GYROTRON is a new type of microwave device employing the electron cyclotron maser mechanism. It ideally consists of an ensemble of monoenergetic electrons following helical trajectories around the lines of an axial magnetic field inside a fast wave structure such as a metallic tube or waveguide. The physical mechanism responsible for the radiation in the gyrotrons has its origin in a relativistic effect. Initially, the phases of the electrons in their cyclotron orbits are random, but phase bunching can occur because of the dependence of electron cyclotron frequency on the relativistic electron mass. Those electrons that lose energy to the wave become lighter, rotate faster, and, hence, accumulate phase lead, while those electrons that gain energy from the wave become heavier, rotate slower, and accumulate phase lag. This can result in phase bunching such that the electrons radiate coherently and amplify the wave. Energy transfer from the electrons to the wave is optimized when $\omega - k_z v_{z0} - s\Omega_c \geqslant 0$, where ω, k_z, v_{z0}, s, and Ω_c, are, respectively, the wave frequency, axial wave number, axial electron veloc-

0018-9480/79/0200-0178$00.75 ©1979 IEEE

ity, cyclotron harmonic number, and electron cyclotron frequency. Early descriptions of the physical process are to be found in the works of Twiss [1], Schneider [2], and Gapanov [3], while a detailed comparison between this (relativistic) azimuthal bunching process and the more familiar (nonrelativistic) axial bunching process has been carried out recently by Chu and Hirshfield [4]. The first deliberate experimental study of the cyclotron maser instability was made by Hirshfield and Wachtel [5]. Prior to the publication of [5], Chow and Pantell [6] reported a cyclotron resonance backward wave oscillator in which the mechanism of radiation was attributed to axial electron bunching. However, in light of the comparative study in [4], their observation was more likely due to the cyclotron maser instability. An extensive summary of the works on cyclotron maser can be found in recent review papers [7], [8].

The gyrotron emits radiation near the frequency $\omega = \Omega_c + k_z v_{z0}$, so the wavelength is determined primarily by the strength of the applied magnetic field and is not restricted necessarily by the dimensions of a resonant structure. Thus unlike most other microwave tubes, the internal dimensions of the device may possibly be large compared to the wavelength, and high power handling capability becomes compatible with operation at millimeter and submillimeter wavelengths. Indeed, the highest recorded millimeter wave power, both peak and average, has been attained in gyrotron devices. The high peak powers were achieved in a series of experiments using intense relativistic electron beams ($V \sim 1$ MV, $I \sim 30$ kA) and powers achieved include 900 MW at $\lambda = 4$ cm[9], 350 MW at $\lambda = 2$ cm[10], 8 MW at $\lambda = 8$ mm[11], and 2 MW at $\lambda = 4$ mm[11]; however, efficiency of converting electron beam energy to EM radiation was only ~ 1 percent. On the other hand, the high average powers were generated with high efficiency and with current and voltage levels similar to those in conventional microwave tubes; thus the high average power work leads directly to practical devices.

The initiative in developing a high average power gyrotron was first taken by workers at the Gorkii State University (U.S.S.R.) [12], [13]. The key to achieving efficient devices was careful design of the electron gun. In the Gorkii studies, a crossed field "magnetron injection gun" was used to launch an annular electron beam with a large fraction of energy transverse to the axis and with minimum energy spread. Work on nonuniform cross-section open resonators to optimize beam-wave coupling has also taken place [13]. All together, these developments have led to the demonstration of a technological breakthrough in CW millimeter wave generation. Using a superconducting magnet, Zaytsev *et al.* [12] have generated the following CW powers: 12 kW at $\lambda = 2.78$ mm with 31-percent efficiency; 2.4 kW at $\lambda = 1.91$ mm with 9.5-percent efficiency, and 1.5 kW at $\lambda = 0.92$ mm with 6.2-percent efficiency. Other impressive results by Soviet workers include the operation of a second-harmonic device in a magnetic field of only 6 kG which produced at

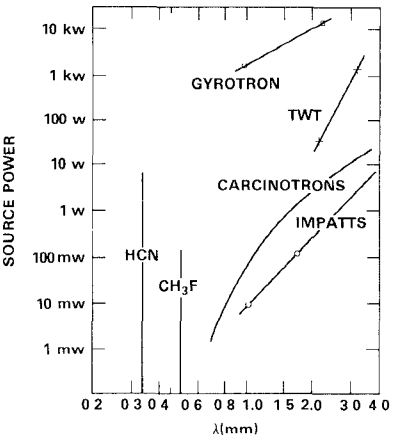

Fig. 1. State-of-art CW power sources.

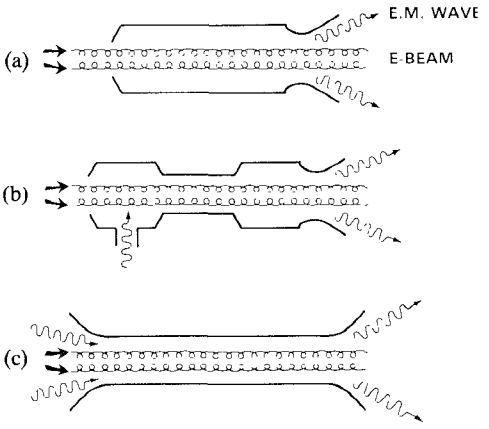

Fig. 2. Type of gyrotrons. (a) Gyromonotron oscillator. (b) Gyroklystron amplifier. (c) Gyro-TWT amplifier.

$\lambda = 9$ mm a CW power of 10 kW with 40-percent efficiency [13]. Fig. 1 compares these results with CW power available from other microwave devices; an advance in CW power capability by 3 to 5 orders of magnitude is clearly indicated.

The Soviet gyrotrons have operated as oscillators using a single resonant cavity as the RF structure. However, the gyrotron process lends itself to the use of a variety of RF structures [8] and can operate as an amplifier as well as an oscillator. In Fig. 2, schematics of three types of gyrotrons are sketched. The gyromonotron in Fig. 2(a) corresponds to the Soviet oscillator configuration. Fig. 2(b) shows the two-cavity gyroklystron amplifier which induces a transverse phase bunching in an input cavity, allows the bunching to continue ballistically between cavities, and then converts transverse electron energy to wave energy in an output cavity. Operation of such a device was reported in an early experiment by Wachtel and Hirshfield [14] and, recently, by Jory [15].

A third type of gyrotron, on which this paper focuses, is the gyrotron traveling wave amplifier (gyro-TWA, Fig. 2(c)). This device is especially uncomplicated in that the RF structure is a simple waveguide. It has a clear advan-

tage in handling high power since the field strengths encountered for a given power level will be much lower in a traveling wave device than in a device employing resonant cavities. Also, superior bandwidth and tunability characteristics are expected. The operation of a gyro-traveling wave amplifier was demonstrated in an experiment using an intense relativistic electron beam [16]. A gain of 16 dB (1.1 dB/cm) was achieved at 8.6 GHz with a bandwidth of ~5 percent and an output power of 4 MW; there was also indication of octave-like tunability through changing the magnetic field in step with the input frequency. However, efficiency in this first gyro-TWA was low in part because of poor beam quality.

On the theoretical side, analytical and numerical studies [17]–[27] of the gyromonotron configuration have appeared frequently in literature and have provided considerable physical insight into the operation of gyromonotrons. These studies have concentrated mostly either on the fundamental cyclotron harmonic interaction or on specialized systems. Recently, a general analysis of the gyromonotron operation at all harmonics of the cyclotron frequency has been carried out [28]. Analytical studies of the gyroklystron configuration has hitherto been lacking. However, numerical modeling [15], [29] has yielded useful information concerning the beam-wave coupling, small signal gain, device efficiency, and stability conditions. For the gyro-TWA configuration, several linear and nonlinear theories [4], [30]–[33] have been reported in recent years. While the basic physical processes have been carefully analyzed in these papers, questions concerning the actual operation of such devices (e.g., parameter optimization, bandwidth, etc.) have not yet been addressed.

This paper presents analytical and simulation studies of a gyro-TWA device operating on the TE_{01} waveguide mode and the fundamental electron cyclotron harmonic. In contrast to previous analyses, our emphasis here will be on the applied aspects of the theory developed, and, in particular, we detail the procedures involved in the design of a highly efficient gyro-TWA device. Hence, methods of parameter optimization and bandwidth calculation have been considered in detail. Operational characteristics such as dependence of efficiency on the electron energy and magnetic field and dependence of bandwidth and power gain on the magnetic field have also been obtained and schematically presented. Although our design is based on the point of maximum efficiency, these characteristic curves are capable of yielding designs based on other criteria such as maximum bandwidth.

II. Design Criteria and Theoretical Approaches

The methods presented here for parameter optimization are generally applicable to gyro-TWA's. As an illustration, we will consider a particular example, namely, a gyro-TWA aimed at the laboratory production of 340-kW (CW or pulsed) power at a frequency of 35 GHz. Wave amplification results from the interaction between the TE_{01} circular waveguide mode

$$\omega^2 - k_z^2 c^2 - \omega_c^2 = 0 \tag{1}$$

and the fundamental cyclotron harmonic of the beam

$$\omega - k_z v_{z0} - \Omega_c = 0 \tag{2}$$

where ω_c is the cutoff frequency of the TE_{01} mode, $\Omega_c \equiv \Omega_e/\gamma_0$, $\Omega_e \equiv e$ B/m, and $\gamma_0 \equiv [1-(v_{\perp 0}^2+v_{z0}^2)/^2]^{-1/2}$.

The principal design criterion is to attain high efficiency. To achieve this, it is desirable to select the magnetic field such that the two curves represented by (1) and (2) intersect at a grazing or near grazing angle in the (ω, k_z) plane, i.e., with the group velocity $(k_z c^2/\omega)$ of the waveguide mode nearly equal to the beam velocity (v_{z0}). The reason for such a choice will become evident.

It is proposed to couple the RF structure designed here with a "magnetron injection gun" of the type used in the Gorkii studies so that an electron beam can be provided with sufficiently high quality to satisfy the design assumptions.

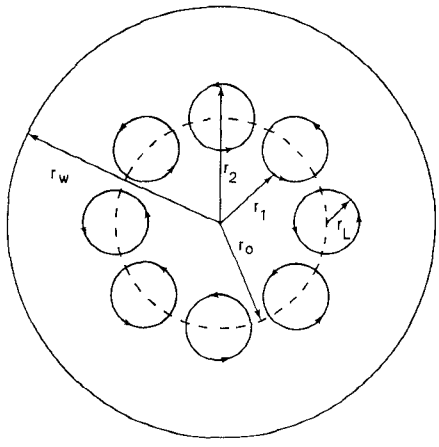

Fig. 3. Cross-sectional view of the gyro-TWA model. The applied magnetic field (not shown) points toward the reader. The electrons are monoenergetic and all have the same Larmor radius r_L. Guiding centers of all electrons are uniformly distributed on the circle of constant radius r_0.

Fig. 3 shows the theoretical model of such a beam-waveguide system. It consists of an annular electron beam propagating with uniform velocity v_{z0} in a circular cross-section waveguide of radius r_w. The system is immersed in an external magnetic field $B_0 e_z$ oriented along the axis of the waveguide. We assume that all electrons have the same perpendicular velocity $v_\perp$. Under the influence of the external magnetic field, the electrons gyrate at the frequency Ω_c and with the Larmor radius $r_L \equiv v_{\perp 0}/\Omega_c$. We assume that the guiding centers of all electrons are uniformly distributed on the surface of constant radius r_0. Thus the beam inner radius (r_1) and outer radius (r_2) are $r_1 = r_0 - r_L$ and $r_2 = r_0 + r_L$.

In this model, we have assumed a thin (thickness $= 2r_L$) monoenergic electron beam. Our recent computer simula-

tion [34] of a carefully designed electron gun shows that a beam with thickness $\leqslant 2.3 r_L$ and energy spread $\ll 1$ percent can be achieved (see Section V).

Calculations of the optimum operating parameters have been based on two independent approaches. First, a linear analytical treatment of the beam-wave interaction has been used to calculate the linear wave frequency, growth rate, and to determine the optimum beam position and wavenumber. As in earlier analyses [31]–[33], the presence of the beam is treated as a perturbation to the waveguide. However, the problem has now been formulated in the realistic cylindrical geometry rather than the idealized parallel plate geometry previously adopted. This improvement in modeling is of considerable importance, since efficiency is a sensitive function of quantities which depend on geometrical factors. A second improvement in modeling is that we treat the electron guiding center radius r_0 as a variable parameter, while in earlier parallel-plate models [31]–[33], the guiding centers were centrally located between the plates. This improvement gives us the means to optimize the beam-wave coupling with respect to r_0.

For generality, all the calculations have been done in the beam frame (i.e., the reference frame in which the beam axial velocity is zero). Furthermore, the following normalization procedures are introduced, through which the waveguide radius r_w is scaled out of the problem:

$$\text{length normalized to } r_w \tag{3}$$

$$\text{frequency normalized to } c/r_w \tag{4}$$

$$\text{velocity normalized to } c \tag{5}$$

$$\text{electric and magnetic field normalized to } mc^2/er_w \text{ and } mc/er_w, \text{ respectively.} \tag{6}$$

The results obtained are thus applicable to any waveguide radius r_w and for any beam axial velocity v_{z0} by the appropriate transformations. In Appendix A, we have included the transformation formulas for conversion from beam frame to lab frame quantities and from dimensionless to physical units.

To maintain a clear distinction between lab frame, beam frame, normalized, and physical quantities, the following notation has been adopted.

1) Beam frame quantities are denoted by primed symbols (e.g., γ_0'); laboratory frame quantities are unprimed (e.g., γ_0).

2) Normalized dimensionless quantities are denoted by a bar (e.g., $\bar{\Omega}_c$). Unbarred symbols represent either physical quantities (e.g., Ω_c) or naturally dimensionless ones (e.g., γ_0).

The derivation of the linear dispersion relation is lengthy but straightforward. Since the methods are analogous to those described in detail by Ott and Manheimer [31], only the result will be presented here.

The normalized dispersion relation for the excitation of the TE_{01} mode at the fundamental electron cyclotron harmonic (expressed in beam frame) is

$$\bar{\omega}'^2 - \bar{k}_z'^2 - \bar{\omega}_c^2 = \frac{4\nu'}{\gamma_0' J_0^2(x_1)} \left[- \frac{(\bar{\omega}'^2 - \bar{k}_z'^2)\beta_{\perp 0}'^2 H(x_1\bar{r}_0, x_1\bar{r}_L)}{(\bar{\omega}' - \bar{\Omega}_c')^2} + \frac{\bar{\omega}' Q(x_1\bar{r}_0, x_1\bar{r}_L)}{\bar{\omega}' - \bar{\Omega}_c'} \right] \tag{7}$$

where $x_1 = 3.832$ is the first nonzero root of $J_1(x) = 0$, $\nu' \equiv N' r_e$ is a dimensionless beam density parameter (N' is the total number of electrons per unit length, $r_e \equiv \mu_0 e^2/4\pi m$ is the classical electron radius), $\beta_{\perp 0}' \equiv v_{\perp 0}'/c$, and

$$H(x,y) \equiv [J_1(x) J_1'(y)]^2 \tag{8}$$

$$Q(x,y) \equiv 2H(x,y) + yJ_1'(y)J_1''(y) \cdot \{J_1^2(x)(1 + x^{-2}) + [J_1'(x)]^2\} + 2J_1(x)J_1'(x)J_1'(y)[yJ_1'(y) - J_1(y)]/xy. \tag{9}$$

Note that the primes in (8) and (9) represent, respectively, the first- and second-derivatives of the Bessel function J_1, with respect to its argument. Elsewhere in this paper, the primes indicate beam frame quantity.

In (7), $\bar{r}_0$, $\bar{r}_L$, and $\bar{\omega}_c$ are frame independent quantities. It can be shown easily that the normalized cutoff frequency of the TE_{01} mode, $\bar{\omega}_c$, is numerically equal to x_1.

This analytical work has been complemented by a single-wave numerical simulation code [32]. A Cartesian code of this type was initially developed by Sprangle and Manheimer [33]. It was later refined by Sprangle and Drober [34] and employed to investigate the saturation mechanisms, also in Cartesian geometry. We have constructed a new code, with improved algorithms, in cylindrical geometry. It has been used to simulate the beam-wave interaction processes until the wave reaches saturation. A self-consistent value of the efficiency can, therefore, be determined. The simulation shows two different but simultaneously present saturation mechanisms—depletion of free electron energy and loss of phase synchronism (phase trapping). The first mechanism dominates when the beam energy is only slightly above threshold. Saturation occurs as soon as the beam loses a small amount of energy and the system becomes linearly stable. This mechanism can lead to saturation even in the linear stage. The second mechanism dominates when the beam energy is well above the threshold. Saturation occurs because an average electron loses so much energy that its relativistic cyclotron frequency no longer matches the wave frequency to favor unstable interactions. The values quoted for the efficiency in Section III are those taken from the simulation data. Conservation of energy was monitored in the code and never deviated by more than 0.1 percent. As a cross check, the linear frequency and growth rate obtained from (7) have been compared to the linear stages of the simulation. The agreement between the two approaches was very good (see Section III).

III. Beam Frame Parameter Optimization

As seen from (7), solutions of the problem in the beam frame and in dimensionless units require the specification of five parameters: $\bar{r}_0$, $\bar{k}_z'$, ν', γ_0', and $\bar{\Omega}_c'$. In the present design, we will choose $\bar{r}_0$ and $\bar{k}_z'$ so that the beam–wave coupling, represented by the linear growth rate $\bar{\omega}_i'$, is a maximum with respect to these two parameters. The parameter ν' will be determined from the required output power. With these three parameters specified, the energy conversion efficiency η', defined as the ratio of the final wave energy to the initial beam energy, can be calculated numerically varying the two remaining parameters γ_0' and $\bar{\Omega}_c'$. The point in the $(\gamma_0', \bar{\Omega}_c')$ parameter space where η' peaks will then be chosen for the design.

The first term on the right-hand side (RHS) of (7), proportional to $\beta_{\perp 0}'^2$, is the driving term for the instability. Hence, to maximize the beam–wave coupling with respect to $\bar{r}_0$, we let $\bar{r}_0 = 0.48$ so that $H(x_1\bar{r}_0, x_1\bar{r}_L)$ peaks with respect to $\bar{r}_0$. This is also the radius at which the wave electric field $\bar{E}_\theta'[\sim J_1(x_1\bar{r})]$ peaks. We mention in passing that, for operation at higher cyclotron harmonics, the optimum beam position does not, in general, coincide with the peak of the wave electric field.

The second term on the RHS of (7) imposes a threshold energy on the beam, below which there will be no instability. For most gyrotron devices including the presently designed one, the beam is well above the threshold energy. Hence, this term can be neglected. We expand $\bar{\Omega}_c'$ about a fixed value $\bar{\Omega}_{c0}'$ and expand $\bar{\omega}'$ and $\bar{k}_z'$ about the intersecting point $(\bar{\omega}_0, \bar{k}_{z0}')$ of the two equations

$$\bar{\omega}'^2 - \bar{k}_z'^2 - \bar{\omega}_c^2 = 0 \tag{10}$$

and

$$\bar{\omega}' - \bar{\Omega}_{c0}' = 0. \tag{11}$$

Substituting

$$\bar{\omega}' = \bar{\omega}_0' + \Delta\bar{\omega}'$$
$$\bar{k}_z' = \bar{k}_{z0}' + \Delta\bar{k}_z'$$
$$\bar{\Omega}_c' = \bar{\Omega}_{c0}' + \Delta\bar{\Omega}_c'$$

into (7) and keeping terms to first order in $\Delta\bar{\omega}'$, $\Delta\bar{k}_z'$, and $\Delta\bar{\Omega}_c'$, we obtain

$$\left(\Delta\bar{\omega}' - \frac{\bar{k}_{z0}'}{\bar{\omega}_0'}\Delta\bar{k}_z'\right)\left(\Delta\bar{\omega}' - \Delta\bar{\Omega}_c'\right)^2 = \frac{-2\nu' x_1^2 \boldsymbol{H}\beta_{\perp 0}'^2}{\gamma_0' J_0^2(x_1)\bar{\omega}_0'}. \tag{12}$$

In (12), $\Delta\bar{\omega}' = \Delta\bar{\omega}_r' + i\Delta\bar{\omega}_i'$ is a complex number, while all other quantities are real. Differentiating (12) with respect to $\Delta\bar{k}_z'$, we obtain

$$\frac{d(\Delta\bar{\omega}')}{d(\Delta\bar{k}_z')} = \frac{\bar{k}_{z0}'(\Delta\bar{\omega}' - \Delta\bar{\Omega}_c')}{\bar{\omega}_0'(3\Delta\bar{\omega}' - \Delta\bar{\Omega}_c' - 2\bar{k}_{z0}'\Delta\bar{k}_z'/\bar{\omega}_0)}. \tag{13}$$

Equation (13) shows that if $\bar{k}_{z0}' = 0$, the growth rate $\Delta\bar{\omega}_i'$ is a maximum regardless of the values of $\Delta\bar{k}_z'$ and $\Delta\bar{\Omega}_c'$, i.e., $\Delta\bar{\omega}_i'$ remains a maximum with respect to $\bar{k}_z'$ even with small variations in $\bar{\Omega}_c'$. In comparison, if $\bar{k}_{z0}' \neq 0$, $\Delta\bar{\omega}_i'$ peaks (i.e., the RHS of (13) is real) only when $\Delta\bar{k}_z' = \Delta\bar{\Omega}_c' = 0$. The case $\bar{k}_{z0}' = 0$ thus has the advantage of insuring maximum growth rate (with respect to $\bar{k}_z'$) when the magnetic fields are varied to optimize the efficiency. It implies a grazing intersection of the two curves represented by (10) and (11) (see Fig. 4). This explains why we have chosen a grazing or near grazing intersection for the design.

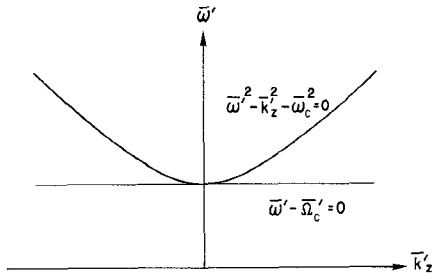

Fig. 4. The vacuum wave guide characteristic curve (10) and the beam characteristic curve (11) in the $(\bar{\omega}', \bar{k}_z')$ plane.

It is convenient to define a new parameter X':

$$X' \equiv \Omega_c'/\omega_c.$$

When the applied magnetic field is such that $X' = 1$, the two curves ((10) and (11)) intersect at an exact grazing angle.

We now consider the choice of ν'. For each value of ν', one can calculate the point in (γ_0', X') space where η' peaks. Given the beam axial velocity v_{z0} in the lab frame, the beam power (P_b) and the output wave power (P_w) at the point of maximum efficiency can then be calculated (see Appendix A, (A5-7)). To specify v_{z0}, we define a lab frame parameter α:

$$\alpha \equiv v_{\perp 0}/v_{z0}.$$

Thus for a fixed value of α, there is a one-to-one correspondence between P_w and ν'. Lengthy calculations are required to deduce ν' from P_w because one might have to scan a range of values for ν' before finding the one that yields the prescribed P_w. In practice, however, one can make a close initial guess for ν' on the basis of the required output wave power, the expected efficiency, and beam energy (see (A5-7)), and then proceed to calculate the optimum γ_0', X', and P_w. If P_w turns out to be too large, for example, by 10 percent, then the next guess for ν', 10 percent smaller, can be very accurate because the relation between P_w and ν' is almost linear. If there is an acceptable range of P_w, the initial guess of ν' usually suffices.

The choice for the velocity ratio α is guided by two considerations—having as much energy in the perpendicular gyromotion as possible and minimizing the beam temperature spread. The second consideration sets an upper limit on α. Our electron gun simulation code [34] showed that for $\alpha > 1.5$, the beam temperature began to increase rapidly and was no longer suitable. The required output wave power is ~300 kW, which corresponds to

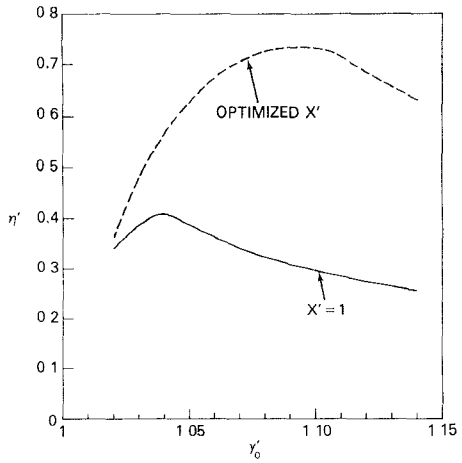

Fig. 5. η' versus γ_0' for grazing intersection case ($X'=1$, solid curve) and for optimized near grazing intersection case ($X' \leqslant 1$, dashed curve). A point on the dashed curve $\eta'(\gamma_0', X')$ is obtained by varying X' but keeping γ_0' fixed until $\eta(\gamma_0', X')$ reaches a maximum, as illustrated in Fig. 6. The peak of the dashed curve is therefore the peak of η' in the (γ_0', X') parameter space. The parameters used for this figure are $\bar{r}_0=0.48$, $\nu'=0.002$, and $\bar{k}_z'=0$.

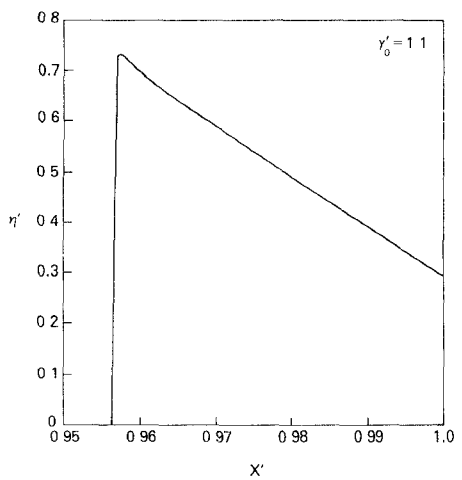

Fig. 6. Efficiency η' versus X' for $\gamma_0'=1.1$, $\bar{r}_0=0.48$, $\nu'=0.002$, and $\bar{k}_z'=0$.

$\nu' \cong 0.002$, if we assume $\gamma_0' \cong 1.1$ and a 45 percent efficiency. Thus we let $\nu'=0.002$ be our initial guess. We now present the calculations that lead to the optimized γ_0', X', and P_w for the initially chosen ν'. The calculated optimum P_w (340 kW) turns out to be about 11 percent larger than expected, but falls in the acceptable range.

With ν' specified at $\nu'=0.002$, the efficiency η' has been calculated in a two-parameter space (γ_0', X'). The results are summarized in Figs. 5 and 6. Fig. 5 shows two plots of η' versus γ_0'. The solid curve represents the efficiency for grazing interaction ($X'=1$). It predicts a maximum efficiency $\eta' \cong 42$ percent at $\gamma_0'=1.04$. The dashed curve shows the efficiency as a function of γ' but for an optimized value of X'. The peak efficiency is now $\eta' \cong 73$ percent at $\gamma_0'=1.10$ and $X' \cong 0.957$. It is interesting to note that the optimization in X' shifts the point of maximum efficiency to higher γ_0' than found for grazing interaction. Decreasing X' from 1 has the effect of delaying phase

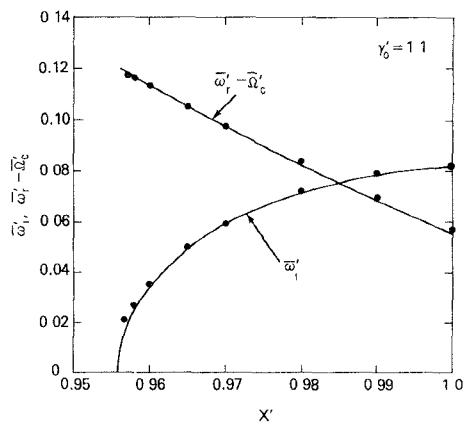

Fig. 7. Growth rate $\bar{\omega}_i'$ and frequency shift $\bar{\omega}_r'-\bar{\Omega}_c'$ versus X' for $\gamma_0'=1.1$, $\bar{r}_0=0.48$, $\nu'=0.002$, and $\bar{k}_z'=0$. $\bar{\omega}_r'$, and $\bar{\Omega}_c'$ are, respectively, the wave frequency and beam electron cyclotron frequency.

trapping [14], which is one of the two mechanisms responsible for saturation. Since phase trapping is more dominant at higher γ_0', this qualitatively explains why the efficiency peak moves to higher γ_0' with magnetic mismatching. To determine quantitatively the value of γ_0' where the efficiency peaks, a thorough search of the (γ_0', X) parameter space was required.

It can be seen in Fig. 5 that at the value of γ_0' for which the maximum efficiency was found, a small variation in X' from 1.0 to 0.96 caused a large change in the efficiency from 30 to 70 percent. To further illustrate the sensitivity of the efficiency as a function of X', a graph of η' versus X' is shown in Fig. 6 for $\gamma_0'=1.10$, the value corresponding to peak efficiency. It can be seen in Fig. 6 that η' is a sensitive function of X'. It increases sharply as X' is decreased from unity and then falls precipitously if X' is reduced too much. This occurs because, for too low a value of X', the system becomes linearly stable. We would like to stress that for an experiment to operate near the peak value of η', it is essential to control parameters such as magnetic field, beam voltage, and driver frequency within an accuracy $\leqslant 1$ percent.

Fig. 7 shows the growth rate $(\bar{\omega}_i')$ and the difference between wave frequency $(\bar{\omega}_r')$ and electron cyclotron frequency $(\bar{\Omega}_c')$ as a function of X' for the same parameters as used in Fig. 6. Solid curves are calculated from (7) and the solid data points are taken from the simulation runs. The agreement between analytical and simulation results is found to be very good for the runs shown in this figure as well as for all other runs. From Figs. 6 and 7, we observe that when the efficiency approaches a maximum as a result of varying X', the growth rate approaches zero. Too low a growth rate is clearly undesirable. However, as one moves slightly away from the peak efficiency, the growth rate increases rapidly. Some compromise must be made between growth rate and efficiency in selecting the operating point. For the designed amplifier, we have chosen the point $X'=0.96$ where the efficiency is $\eta'=70$ percent, only 3 percent below the peak value. As will be shown, this point corresponds to a reasonably high power

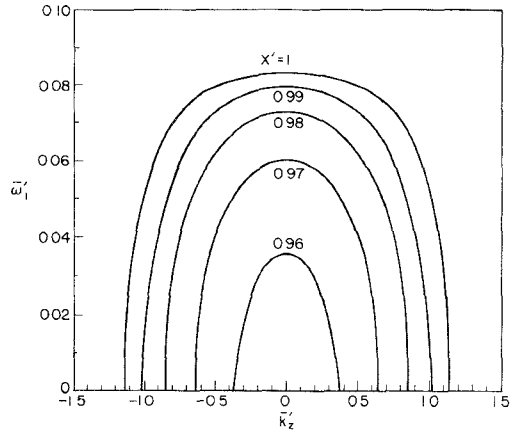

Fig. 8. Growth rate versus wavenumber for $\nu'=0.002$ $\bar{r}_0=0.48$, $\gamma_0'=1.1$, and several values of X'.

TABLE I
FORMULAS FOR TRANSFORMATION FROM BEAM FRAME INTO LAB FRAME AND FOR CONVERTING NORMALIZED QUANTITIES INTO PHYSICAL QUANTITIES

Beam Frame Normalized Quantities	Lab Frame Normalized Quantities	Lab Frame Physical Quantities
ν'	$\nu=\gamma_z\nu'$	ν (dimensionless)
γ_o'	$\gamma_o=\gamma_z\gamma_o'$	γ_o (dimensionless)
η'	$\eta=\dfrac{\eta'\gamma_z(\gamma_o'-1)(1+\bar{k}_z'\beta_{zo}/\bar{\omega}')^2}{\gamma_z\gamma_o'-1}$	η (dimensionless)
$\bar{\omega}_r'$	$\bar{\omega}_r=\gamma_z(\bar{\omega}_r'+\bar{k}_z'\beta_{zo})$	$\omega_r=\bar{\omega}_r c/r_w$
$\bar{\omega}_i'$	$\bar{\omega}_i=\bar{\omega}_i'/\gamma_z$	$\omega_i=\bar{\omega}_i c/r_w$
$\bar{k}_z'$	$\bar{k}_z=\gamma_z(\bar{k}_z'+\beta_{zo}\bar{\omega}_r')$	$k_z=\bar{k}_z/r_w$
$\bar{\Omega}_e'$	$\bar{\Omega}_e=\bar{\Omega}_e'$	$\Omega_e=\bar{\Omega}_e c/r_w$
$\bar{r}_L'$	$\bar{r}_L=\bar{r}_L'$	$r_L=\bar{r}_L r_w$
$\bar{r}_o'$	$\bar{r}_o=\bar{r}_o'$	$r_o=\bar{r}_o r_w$

gain (2 dB/cm). The other parameters corresponding to this point are: $X'=0.96$, $\nu'=0.002$, $\bar{r}_0=0.48$, $\gamma_0'=1.1$, $\bar{k}_z'=0$, $\bar{\omega}_r'=3.791$, and $\bar{\omega}_i'=0.0342$.

IV. Power Gain and Bandwidth

Information concerning the power gain and bandwidth is contained in the dispersion relation (7), which gives the growth rate and the width of the unstable spectrum in the beam frame. Fig. 8 shows some typical plots of $\bar{\omega}'$ versus $\bar{k}_z'$ for $\nu'=0.002$, $\bar{r}_0=0.48$, $\gamma_0'=1.1$, and several values of X'. The beam frame normalized growth rate ($\bar{\omega}_i'$) can be readily converted into the lab frame physical growth rate (ω_i) by the use of the relevant formula in Table I. To calculate the total power gain (G) and the power gain per unit length (g), we consider a gyro-TWA device characterized by a linear growth rate ω_i and interaction length L. At the *linear* growth rate, the wave power amplification is given by

$$P_{\text{out}}=P_{\text{in}}\exp(2\omega_i\tau) \tag{14}$$

where $\tau\equiv L/v_{z0}$, v_{z0} is the beam axial velocity and P_{in}, P_{out} are, respectively, the input and output wave powers. In terms of G, P_{in} and P_{out} are related through

$$P_{\text{out}}=10^{G/10}P_{\text{in}}. \tag{15}$$

From (14) and (15), we obtain the total power gain

$$G=20\omega_i\tau/\ln 10\cong 8.7\omega_i\tau \text{ dB} \tag{16}$$

and the power gain per unit length

$$g\cong 8.7\omega_i/v_{z0}. \tag{17}$$

To find the bandwidth, we let ω_i^m and ω_i^h be the growth rates which yield the maximum power and half of the maximum power, respectively, and let G^m and G^h be the corresponding power gains. By definition, G^m and G^h are related through

$$G^h=G^m-10\log 2. \tag{18}$$

Equations (16) and (18) give the ratio of ω_i^h to ω_i^m:

$$R=\omega_i^h/\omega_i^m=G^h/G^m=1-10\log 2/G^m. \tag{19}$$

The ratio R calculated from (19) is frame independent (see the transformation formula for ω_i in Table I). It determines the half-power points in the $\bar{\omega}_i'$ versus $\bar{k}_z'$ plot (see Fig. 8) and, therefore, the width $\Delta\bar{k}_z'$ between the half-power points. Through a Lorentz transformation, we obtain the lab frame bandwidth

$$\Delta\omega/\omega\cong\beta_{z0}\Delta\bar{k}_z'/x_1 \tag{20}$$

where $\beta_{z0}=v_{z0}/c$, and we have assumed $\bar{k}_z'=0$ at the center of the band (corresponding to grazing or near grazing intersection).

Fig. 9 plots the bandwidth ($\Delta\omega/\omega$) as a function of X' for $\gamma_0'=1.1$, $\alpha=1.5$, $\nu'=0.002$, $\bar{r}_0=0.48$, and $G=10$, 20, and 30. Comparing Figs. 7 and 9, we note that higher efficiency corresponds to lower X' and, hence, lower bandwidth.

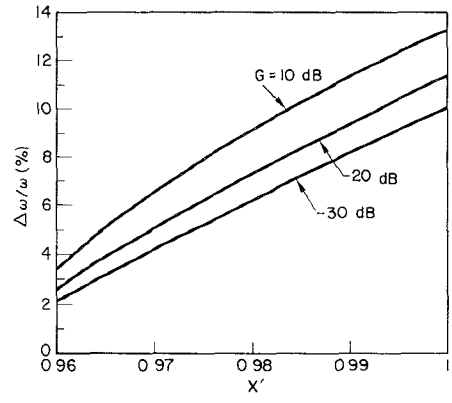

Fig. 9. Bandwidth versus X' for $\alpha=1.5$, $\nu'=0.002$ $\bar{r}_0=0.48$, $\gamma_0'=1.1$, and several values of total power gain G.

V. Conversion of Beam Frame Optimum Parameters into Design Parameters

To convert the beam frame optimum parameters into actual design parameters, two pieces of information are required: 1) the beam axial velocity (in a lab frame), which can be calculated from the previously specified

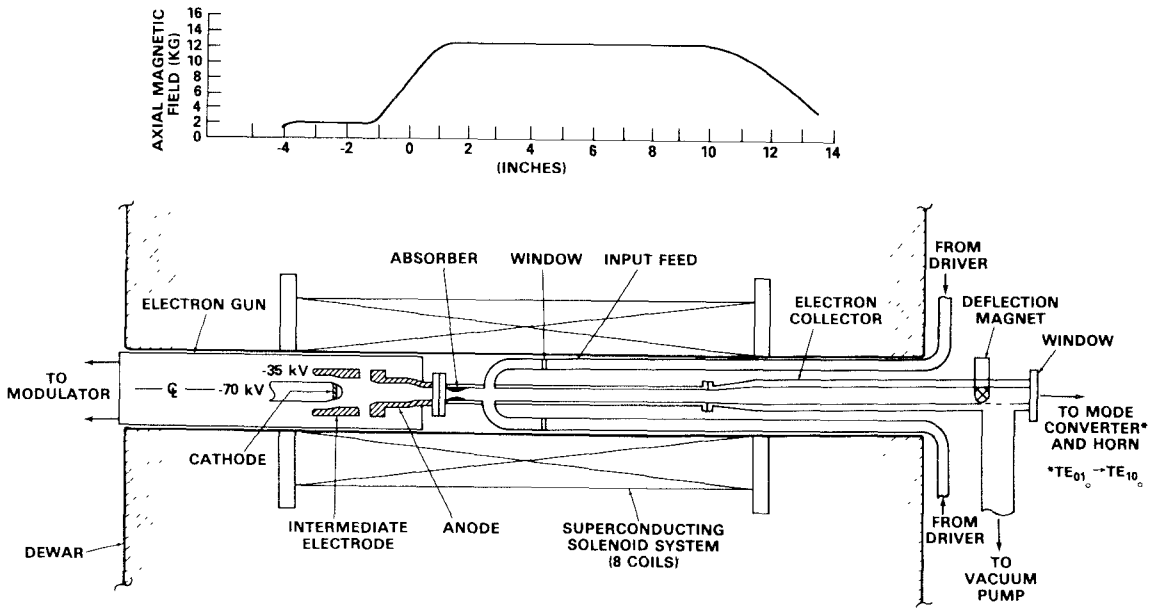

Fig. 10. Configuration of the designed gyro-TWA.

TABLE II
EFFICIENTLY OPTIMIZED OPERATING PARAMETERS FOR THE NRL GYROTRON TWA $\alpha = 1.5, f = 35$ GHz ($\lambda = 8.57$ mm)

ν (density parameter)	2.076×10^{-3}
V (electron energy)	70.82 keV
I_b (beam current)	9.48 Amp
η (efficiency)	51.0%
P_b (beam power)	671.5 kW
P_w (wave power)	342.5 kW
B_0	12.87 kG
k_z	1.96 cm^{-1}
r_w	5.37 mm
r_0	2.52 mm
r_f	0.61 mm
r_1	1.91 mm
r_2	3.13 mm
$v_{\perp 0}/c$	0.401
v_{z0}/c	0.268
g (power gain)	2.0 dB/cm
bandwidth (for $G = 20$)	2.6%

value of α, and 2) the waveguide radius, which is determined from the desired wave frequency, $f = 35$ GHz (see Appendix A, (A-4)).

Using the conversion formulas tabulated in Appendix A, we have converted the optimum parameters obtained in Section III into the design parameters for a 35-GHz 340-kW gyro-TWA. They are shown in Table II.

The experimental configuration which was based on these design parameters is shown in Fig. 10. The entire device is placed within the bore of a superconducting magnet. This allows precise shaping of the magnetic field over the entire electron beam. Such control is essential because of the great impact small changes in the magnetic field have on both the device efficiency and the operation of the electron gun. The magnetic field profile shows a carefully designed compression region required to obtain a beam with the proper velocity ratio α. After being compressed, the beam enters a uniform magnetic field region where the cyclotron maser mechanism operates. An external driver generates a RF signal which is injected at two azimuthal positions at the left end of the drift tube so as to launch a TE_{01} wave. The use of an absorber ensures that the wave can propagate in only one direction so as to prevent oscillations. Amplification occurs in the uniform field region to the right of the RF injection point. Beyond this region, the electron beam is collected at the wall as the magnetic field falls off. Stray electrons are deflected by a small magnet. The RF signal continues down the drift tube and exits at the window.

VI. Discussion and Conclusion

At this time, there exists no comprehensive theory detailing the effects of beam temperature on the efficiency of gyro-TWA's. It is possible, however, on the basis of the condition of phase synchronism, to derive the following qualitative condition for the validity of the cold beam approximation [35] (expressed in the lab frame):

$$\bar{k}_z \delta\beta_z + \bar{\Omega}_c \delta\gamma \ll \left[\frac{2\nu x_1 H \beta_{\perp 0}^2}{\gamma_0 J_0^2(x_1)} \right]^{1/3} \tag{21}$$

where $\delta\beta_z$ is the axial velocity spread normalized to the speed of light and $\delta\gamma$ is the energy spread. A numerical simulation has been made of the NRL electron gun [35] (see Fig. 10 for its configuration). The beam produced in the simulation is almost monoenergetic. Typically, the energy spread is much smaller than 1 percent. So, contribution to the left-hand side (LHS) of (21) comes mainly from the $\delta\beta_z$ term, which is caused by a velocity pitch angle spread. Neglecting the second term on the LHS of (21) and using the parameters in Table II, we obtain

$$\delta\beta_z \ll 0.2. \tag{22}$$

A typical value for $\delta\beta_z$ in the simulation runs is 0.02. Thus the inequality in (22) is well satisfied and the cold beam approximation adopted in our theory appears to be realistic based on the simulation studies of the electron gun.

In conclusion, we have formulated the linear cyclotron maser theory and a numerical simulation code in cylindrical geometry and obtained various operational characteristics for a gyro-TWA device. We show, through an example, how the parameters of a gyrotron device are optimized to achieve high efficiencies. The choice of beam position r_0 and wave number k_z are based on the condition of maximum linear beam–wave coupling. The beam density parameter ν is determined from the required power level. Finally, the specification of the lab frame beam energy γ_0' and the cyclotron frequency parameter X' is based on extensive numerical calculation of efficiency in the (γ_0', X') parameter space.

Sensitivity of the efficiency to small variations in the relativistic electron cyclotron frequency requires that the beam energy and the external magnetic field be controllable within an accuracy of $\leqslant 1$ percent.

Appendix A
Conversion Formulas

Theoretical calculations in the present work are carried out in beam frame, and parameters are normalized according to (3)–(6). In this Appendix, we tabulate the formulas needed to convert beam frame normalized quantities to lab frame physical quantities. Column 2 of Table I converts the beam frame normalized quantities in column 1 to lab frame normalized quantities. The information needed for the conversion is the axial velocity v_{z0} (in lab frame) which defines the quantity γ_z in column 2:

$$\gamma_z \equiv \left[1-\beta_{z0}^2\right]^{-1/2}$$

where $\beta_{z0}=v_{z0}/c$.

Formulas presented in column 2 are based on the Lorentz transform. Derivations are obvious except for items 3–6.

To derive the conversion formula for the efficiency, we note that the EM field energy per unit length is

$$W_f = \frac{KB_z^2\omega^2}{8\pi\omega_c^2} \tag{A1}$$

where K is a geometrical factor, B_z is the axial magnetic field component of the amplified wave, and ω_c is the waveguide cutoff frequency.

The injected beam energy per unit length is

$$W_b = N(\gamma_0-1)mc^2$$

where N is defined in the text.

The lab frame efficiency (η) can, therefore, be written

$$\eta = \frac{W_f}{W_b} = \frac{KB_z^2 mc^2\omega^2}{8\pi\omega_c^2 N(\gamma_0-1)}. \tag{A2}$$

In (A2) K, B_z, and ω_c are all frame independent quantities.

The beam frame efficiency (η') is also expressed by (A2) with ω, N, and γ_0 replaced by ω', N', and γ_0', respectively. Thus

$$\frac{\eta}{\eta'} = \frac{\omega^2 N'(\gamma_0'-1)}{\omega'^2 N(\gamma_0-1)}. \tag{A3}$$

Since $\omega=\gamma_z(\omega'+k_z'v_{z0})$, $\gamma_0=\gamma_z\gamma_0'$, and $N=\gamma_z N'$, substitution of these relations into (A3) yields item 3 in Table I.

To derive the conversion formulas for ω_r, ω_i, and k_z, we assume that the wave fields vary as $\exp(-i\omega' t'+ik_z'z')$ in the beam frame. Since t' and z' can be expressed in terms of lab frame t and z as $t'=\gamma_z(t-v_{z0}z/c^2)$ and $z'=\gamma_z(z-v_{z0}t)$, we obtain

$$\begin{aligned}\exp(-i\omega' t'+ik_z'z') &= \exp\left[-i(\omega_r'+i\omega_i')\gamma_z\left(t-v_{z0}z/c^2\right)\right.\\ &\quad \left.+ik_z'\gamma_z(z-v_{z0}t)\right]\\ &= \exp\left[-i\gamma_z(\omega_r'+k_z'v_{z0})t\right.\\ &\quad +i\gamma_z\left(k_z'+\omega_r'v_{z0}/c^2\right)z\\ &\quad \left.+\gamma_z\omega_i' t-\frac{\gamma_z\omega_i' v_{z0}}{c^2}z\right].\end{aligned}$$

Thus the wave, viewed from the lab frame, has the following frequency (ω_r) and wave number (k_z):

$$\omega_r = \gamma_z(\omega_r'+k_z'v_{z0})$$
$$k_z = \gamma_z\left(k_z'+\omega_r'v_{z0}/c^2\right)$$

and, if one follows a beam segment (i.e., let $z=v_{z0}t$), one observes a growth rate given by

$$\omega_i = \gamma_z\omega_i'\left(1-v_{z0}^2/c^2\right)=\omega_i'/\gamma_z.$$

Column 3 converts the lab frame normalized quantities in column 2 to lab frame physical quantities. The conversion formulas are based on (3)–(5) in the main text. The information needed at this step is the waveguide radius r_w, which can be determined from the desired wave frequency through

$$r_w = \bar{\omega}_r c/2\pi f \tag{A4}$$

where $\bar{\omega}_r$ is the calculated wave frequency (normalized) and f is the desired wave frequency in hertz.

From the lab frame physical quantities in column 3, we can derive the beam current (I_b), beam power (P_b), and the maximum output wave power (P_w):

$$I_b = \nu mc^2 v_{z0}/e = 1.707\times 10^4 \nu\beta_{z0}\ \text{A} \tag{A5}$$

$$P_b = I_b(\gamma_0-1)mc^2 = 8.535\times 10^6\nu(\gamma_0-1)v_{z0}/c\ \text{kW} \tag{A6}$$

$$P_w = \eta P_b. \tag{A7}$$

Acknowledgment

The authors would like to thank Dr. T. Godlove, Dr. R. Parker, Dr. M. Reed, and Dr. P. Sprangle for many helpful discussions.

REFERENCES

[1] R. Q. Twiss, "Radiation transfer and the possibility of negative absorption in radio astronomy," *Australian J. Phys.*, vol. 11, pp. 564–579, 1958.

[2] J. Schneider, "Stimulated emission of radiation by relativistic electrons in magnetic field," *Phys. Rev. Lett.*, vol. 2, pp. 504–505, 1959.

[3] A. V. Gaponov, "Interaction between electron fluxes and electromagnetic waves in waveguides," *Izv. VUZ., Radiofizika*, vol. 2, pp. 450–462, 1959, and "Addendum," *Izv. VUZ., Radiofizika*, vol. 2, p. 837, 1959.

[4] K. R. Chu and J. L. Hirshfield, "Comparative study of the axial and azimuthal bunching mechanisms in electromagnetic cyclotron instabilities," *Phys. Fluids*, vol. 21, pp. 461–466, 1978.

[5] J. L. Hirshfield and J. M. Wachtel, "Electron cyclotron maser," *Phys. Rev. Lett.*, vol. 12, pp. 533–536, 1964.

[6] K. K. Chow and R. H. Pantell, "The cyclotron resonance backward wave oscillator," *Proc. IRE*, vol. 48, pp. 1865–1870, 1960.

[7] V. A. Flyagin, A. V. Gaponov, M. I. Petelin, and V. R. Yulpatov, "The gyrotron," *IEEE Trans. Microwave Theory Tech.*, vol. MTT-25, pp. 514–521, 1977.

[8] J. L. Hirshfield and V. L. Granatstein, "The electron cyclotron maser—An historical survey," *IEEE Trans. Microwave Theory Tech.*, vol. MTT-25, pp. 522–527, 1977.

[9] V. L. Granatstein, M. Herndon, P. Sprangle, Y. Carmel, and J. A. Nation, "Gigawatt microwave emission from an intense relativistic electron beam," *Plasma Phys.*, vol. 17, pp. 23–28, 1975.

[10] V. L. Granatstein, M. Herndon, R. K. Parker, and S. P. Schlesinger, "Strong submillimeter radiation from intense relativistic electron beams," *IEEE Trans. Microwave Theory Tech.*, vol. MTT-22, pp. 1000–1005, 1974.

[11] M. Friedman and M. Herndon, "Emission of coherent microwave radiation from a relativistic electron beam propagating in a spatially modulated field," *Phys. Fluids*, vol. 16, pp. 1982–1995, 1973.

[12] N. I. Zaytsev, T. B. Pankratova, M. I. Petelin, and V. A. Flyagin, "Millimeter and submillimeter waveband gyrotrons," *Radio Eng. Electron. Phys.*, vol. 19, pp. 103–107, May 1974.

[13] D. V. Kisel', G. S. Korablev, V. G. Navel'yev, M. I. Petelin, and S. E. Tsimring, "An experimental study of a gyrotron, operating at the second harmonic of the cyclotron frequency, with optimized distribution of the high frequency field," *Radio Eng. Electron. Phys.*, vol. 19, pp. 95–100, Apr. 1974.

[14] J. M. Wachtel and J. L. Hirshfield, "Interference beats in pulse-stimulated cyclotron radiation," *Phys. Rev. Lett*, vol. 17, pp. 348–351, 1966.

[15] H. R. Jory, "Millimeter wave gyrotron development—Phase I," Varian Ass. Inc., Rep. No. RADC-TR-77-210, June 1977, unpublished.

[16] V. L Granatstein, P. Sprangle, M. Herndon, R. K. Parker, and S. P. Schlesinger, "Microwave amplification with an intense relativistic electron beam," *J. Appl. Phys.*, vol. 46, pp. 3800–3805, 1975.

[17] J. L. Hirshfield, I. B. Bernstein, and J. M. Wachtel, "Cyclotron resonance interaction of microwaves with energetic electrons," *IEEE J. Quantum Electron.*, vol. QE-1, pp. 237–245, 1965.

[18] T. W. Hsu and P. N. Robson, "Negative absorption from weakly relativistic electrons traversing a Cuccia coupler," *Electron. Lett.*, vol. 1, pp. 84–85, 1965.

[19] A. V. Gaponov, M. I. Petelin, and V. K. Yulpatov, "The induced radiation of excited classical oscillators and its use in high-frequency electronics," *Izv. Vyssh, Ucheb. Zaved., Radiofizi.*, vol. 10, pp. 1414–1453, 1967; also in *Radio Phys. Quantum Electron.*, vol. 10, pp. 794–813, 1967.

[20] G. N. Rapoport, A. K. Nemak, and V. A. Zhurakhovskiy, "Interaction between helical electron beams and strong electromagnetic cavity-fields at cyclotron frequency harmonics," *Radio Eng. Electron. Phys.*, vol. 12, pp. 587–595, 1967.

[21] A. F. Kurin, "Cyclotron maser theory," *Radio Eng. Electron. Phys.*, vol. 14, pp. 1652–1654, 1969.

[22] G. J. Sehn and R. E. Hayes, "Relativistic effect in electron cyclotron transverse-wave devices," *IEEE Trans. Electron Devices*, vol. ED-16, pp. 1077–1078, 1969.

[23] P. A. Lindsay, "Cyclotron-resonance interaction-classical and quantum mechanical treatments compared," in *Proc. 7th Int. Conf. Microwave and Optical Generation and Amplification*, Amsterdam, Holland, Sept. 1970.

[24] B. Kulke, "Limitations on millimeter-wave power generation with spiraling electron beams," *IEEE Trans. Electron Devices*, vol. ED-19, pp. 71–79, 1972.

[25] S. V. Kolosov and A. A. Kurayev, "Comparative analysis of the interaction at the first and second harmonics of the cyclotron frequency in gyroresonance devices," *Radio Eng. Electron. Phys.*, vol. 19, no. 10, pp. 65–73, 1974.

[26] V. L. Bratman and A. E. Tokarev, "On the theory of the relativistic cyclotron-resonance maser," *Izv. Vyssh. Ucheb. Zaved. Radiofiz.*, vol. 17, p. 1224, 1974; also in *Radio Phys. Quantum Electron.*, vol. 17, pp. 932–935, 1974.

[27] M. I. Petelin and V. K. Yulpatove, "Linear theory of a monotron cyclotron-resonance maser," *Radio Phys. Quantum Electron.*, vol. 18, pp. 212–219, 1975.

[28] K. R. Chu, "Theory of electron cyclotron maser interaction in a cavity at the harmonic frequencies," Naval Res. Lab. Memo Rep. No. 3672, *Phys. Fluids*, in press, Dec. 1978.

[29] A. A. Kurayev, F. G. Schevchenko, and V. P. Shestakovich, "Efficiently optimized output cavity profiles that provide a higher margin of gyroklystron stability," *Radio Eng. Electron. Phys.*, vol. 19, no. 5, pp. 96–103, 1974.

[30] A. V. Gaponov and V. K. Yulpatov, "Interaction of helical electron beams with the electromagnetic field in a waveguide," *Radio Eng. Electron. Phys.*, vol. 12, pp. 582–587, 1967.

[31] E. Ott and W. M. Manheimer, "Theory of microwave emission by velocity-space instabilities of an intense relativistic electron beam," *IEEE Trans. Power App. Syst.*, vol. PAS-3, pp. 1–5, 1975.

[32] A. T. Drobot and K. R. Chu, to be published.

[33] P. Sprangle and W. M. Manheimer, "Coherent nonlinear theory of a cyclotron instability," *Phys. Fluids*, vol. 18, pp. 224–230, 1975

[34] P. Sprangle and A. T. Drobot, "The linear and self-consistent nonlinear theory of the electron cyclotron maser instability," *IEEE Trans. Microwave Theory Tech.*, vol. MTT-25, pp. 528–544, 1977.

[35] J. L. Seftor, A. T. Drobot, and K. R. Chu, "An investigation of a magnetron injection gun suitable for use in cyclotron resonance masers," Naval Res. Lab. Memo Rep. No. 3697, to be published.